Linear-optical implementations of the iSWAP and controlled NOT gates based on conventional detectors

Monika Bartkowiak and Adam Miranowicz*

Faculty of Physics, Adam Mickiewicz University, PL-61-614 Poznań, Poland
**Corresponding author: miran@amu.edu.pl*

Received April 20, 2010; revised August 31, 2010; accepted September 3, 2010;
posted September 14, 2010 (Doc. ID 127243); published October 21, 2010

The majority of linear-optical nondestructive implementations of universal quantum gates are based on single-photon resolving detectors. We propose two implementations, which are nondestructive (i.e., destroying only ancilla states) and work with conventional detectors (i.e., those which do not resolve a number of photons). Moreover, we analyze a recently proposed scheme of Wang *et al.* [J. Opt. Soc. Am. B **27**, 27 (2010)] of an optical iSWAP gate based on two ancillae in Bell's states, classical feedforward, and conventional detectors with the total probability of success equal to $\eta^4/32$, where η is detector's efficiency. By observing that the iSWAP gate can be replaced with the controlled NOT gate with additional deterministic gates, we list various possible linear-optical implementations of the iSWAP gate: (i) assuming various ancilla states (unentangled, two-photon, and multiphoton-entangled states) or no ancillae at all, (ii) with or without classical feedforward, (iii) destructive or nondestructive schemes, and (iv) using conventional or single-photon detectors. In particular, we show how the nondestructive iSWAP gate can be implemented with the success probability of $\eta^4/8$ assuming the same ancillae, classical feedforward, and a fewer number of conventional detectors than those in the scheme of Wang *et al.* We discuss other schemes of the nondestructive universal gates using conventional detectors and entangled ancillae in a cluster state, and Greenberger–Horne–Zeilinger and Bell's states giving the success probabilities of $\eta^4/4$, $\eta^6/8$, and $\eta^4/8$, respectively. In the latter scheme, we analyze how detector imperfections (dark counts in addition to finite efficiency and no photon-number resolution) and imperfect sources of ancilla states deteriorate the quantum gate operation.

OCIS codes: 270.0270, 270.5585.

1. INTRODUCTION

In the last decade there has been much interest in probabilistic quantum computing using linear-optical elements and postselection based on counts at photodetectors (see a review in [1] and references therein). These studies have been triggered by the pioneering works of Knill, Laflamme, and Milburn (KLM) [2] and Koashi, Yamamoto, and Imoto (KYI) [3]. Various linear-optical implementations of universal two-qubit gates were proposed including the controlled NOT (CNOT) and controlled sign (CS) gates as listed in Table 1.

Analysis of Table 1 shows that the majority of implementations of the CS/CNOT gates are based on selective (i.e., single-photon or photon-number resolving) detectors, and thus achieving a higher probability of success in comparison to those schemes based on conventional detectors. However, in practical applications the most interesting implementations are those using conventional detectors (also referred to as the bucket detectors) which indicate the presence or absence of photons only.

Surprisingly, there are a very few schemes which are nondestructive and work with conventional detectors (see Table 1). Apart from the proposal of Zou *et al.* [4], there are schemes by Gasparoni *et al.* [5] (scheme 14) and Zhao *et al.* [6] (scheme 15), which are experimental realizations of the modified gate of Pittman *et al.* [7] (scheme 12) without feedforward. In these implementations a quantum encoder (described in Section 4) was used so that the whole setup could realize the nondestructive CNOT gate (with single-photon detectors). However, without having such photon-number resolving detectors for appropriate wavelength, they used conventional detectors in experiments. Moreover, two additional (conventional) detectors were added for the postselection of the output states. So, they only realized a *destructive* version of the nondestructive CNOT gate of Pittman *et al.* [7]. In Sections 3 and 4, we propose two implementations of the *nondestructive* universal gates based on conventional detectors.

In a recent article, Wang *et al.* [8] described a polarization-encoded linear-optical implementation of a nondestructive iSWAP gate using two entangled ancillae in the Einstein–Podolsky–Rosen (EPR) states, classical feedforward, and conventional detectors. The total probability of success of this gate is $P=\eta^4/32$, where η is the detector efficiency, and the power of η corresponds to the number of simultaneously clicking detectors. In this article, we show how to simplify and improve the scheme of Wang *et al.* [8] to obtain the probability of success four times higher and to reduce the number of conventional detectors, while assuming the same ancillae.

The iSWAP, CNOT, and CS are universal gates, so they are formally equivalent, and each of them (together with

Table 1. List of Selected Linear-Optical Implementations of the CS/CNOT Gates, Which Can Directly be Applied to Implement the iSWAP Gate[c]

No.	Author	E/T	Comment	P	Feedforward	Entangled Ancillae	Destructive	Conventional Detector
			I. Unentangled ancillae					
1	KLM [2]	T		$\frac{1}{16}$	No	0	No	No
2	Ralph *et al.* [47]	T	Simplified No. 1	$\frac{1}{16}$	No	0	No	No
3	Knill [29]	T	Improved No. 1	$\frac{2}{27}$	No	0	No	No
4	Pittman *et al.* [34]	E		$\frac{1}{8}$	No	0	Yes[a]	No
5	Pittman *et al.* [34]	T	Modified No. 4	$\frac{1}{4}$	Yes	0	Yes[a]	No
6	Giorgi *et al.* [32]	T	Modified No. 16	$\frac{1}{8}$	Yes	0	No	No
7	Bao *et al.* [33]	E	Modified No. 13	$\frac{1}{8}$	Yes	0	No	No
			II. Entangled ancillae					
8	KLM [2]	T		$\frac{1}{4}$	Yes	EPR	No	No
9	KYI [3]	T		$\frac{1}{16}$	Yes	EPR	No	No
10	KYI [3]	T	Modified No. 9	$\frac{1}{4}$ [b]	Yes	$3\times$EPR	No	No
11	KYI [3]	T	Modified No. 9	$\frac{1}{4}$	Yes	$5\times$EPR	No	No
12	Pittman *et al.* [7]	T		$\frac{1}{16}$	No	EPR	No	No
13	Pittman *et al.* [7]	T	Modified No. 12	$\frac{1}{4}$	Yes	EPR	No	No
14	Gasparoni *et al.* [5]	E	Realization of No. 12	$\frac{1}{16}$	No	EPR	Yes[a]	Yes
15	Zhao *et al.* [6]	E	Realization of No. 12	$\frac{1}{16}$	No	EPR	Yes[a]	Yes
16	Giorgi *et al.* [32]	T	Related to No. 12	$\frac{1}{4}$	Yes	EPR	No	No
17	Zou *et al.* [4]	T	Related to No. 12	$\frac{1}{8}$	Yes	$2\times$EPR	No	Yes
18	Gottesman and Chuang [10]	T		—	Yes	$\|\chi\rangle$	No	—
19	Pittman *et al.* [7]	T	Based on No. 18	$\frac{1}{4}$	Yes	$\|\chi\rangle$	No	No
			III. Without ancillae					
20	Pittman *et al.* [7]	T		$\frac{1}{4}$	No	0	Yes	No
21	Pittman *et al.* [7]	T	Modified No. 20	$\frac{1}{2}$	Yes	0	Yes	No
22	Pittman *et al.* [48]	E	Realization of No. 20	$\frac{1}{4}$	No	0	Yes	No
23	Giorgi *et al.* [32]	T	Related to No. 20	$\frac{1}{4}$	No	0	Yes	No
24	Giorgi *et al.* [32]	T	Modified No. 23	$\frac{1}{2}$	Yes	0	Yes	No
25	Hofmann and Takeuchi [35]	T		$\frac{1}{9}$	No	0	Yes[a]	No
26	Ralph *et al.* [36]	T	Equivalent to No. 25	$\frac{1}{9}$	No	0	Yes[a]	No
27	O'Brien [49]	E	Realization of No. 25, No. 26	$\frac{1}{9}$	No	0	Yes[a]	No
28	Okamoto *et al.* [50]	E	Realization of No. 25, No. 26	$\frac{1}{9}$	No	0	Yes[a]	No
29	Kiesel *et al.* [51]	E	Simplified No. 25, No. 26	$\frac{1}{9}$	No	0	Yes[a]	No
30	Langford *et al.* [52]	E	Equivalent to No. 29	$\frac{1}{9}$	No	0	Yes[a]	No

[a]Measurement of both the control and target bits used for postselection.
[b]Assuming perfect efficiency ($\eta=1$) of detectors.
[c]Key: P—the total probability of success, E/T—experimental/theoretical implementation, $|\chi\rangle$—the Gottesman–Chuang state equivalent to a four-qubit cluster state [10]. See the AppendixA for more explanations.

single-qubit operations) can be used to construct any other gates and quantum circuits. Finding advantages of one universal gate over another can be understood only in terms of their experimental feasibility or specific qubit interactions in studied systems. For example, it is usually much easier to implement the iSWAP gates rather than the CNOT gates in solid-state systems. This is because the iSWAP operation naturally occurs during common solid-state qubit interactions described by the Heisenberg or XY models, while the CNOT operation can be generated from less common Ising interactions. For this reason, efficient quantum-information processing based on the iSWAP gates was studied for solid-state qubits [9]. However, it seems that there is no clear advantage of the linear-optical implementations of the iSWAP gates over other universal optical gates, maybe except some realizations in specific hybrid optical and solid-state systems.

In Section 2, we present simple schemes to decompose the iSWAP gate into the CS or CNOT gate, for which many proposals (see Table 1 and AppendixA) can be readily applied. In particular, by using such schemes together with an implementation of the CS gate by Zou *et al.* [4], which was actually used in [8], one obtains the iSWAP gate with the success probability $P=\eta^4/8$. In Section 3, we discuss other implementations of the iSWAP gate yielding $P=\eta^4/4$ and $P=\eta^6/8$ using as resources the Gottesman–Chuang four-qubit entangled state [10] and a pair of Greenberger–Horne–Zeilinger (GHZ) states, re-

spectively. In Section 4, we propose a scheme using the same resources (including ancillae in the EPR states) as the CS gate of Zou *et al.* [4]. We conclude in Section 5.

2. DECOMPOSITION OF THE iSWAP GATE AND IMPROVED SCHEME OF WANG *et al.*

The iSWAP gate changes an arbitrary pure state of two photon-polarization qubits,

$$|\psi_{\text{in}}\rangle = \alpha_1|HH\rangle + \alpha_2|HV\rangle + \alpha_3|VH\rangle + \alpha_4|VV\rangle, \quad (1)$$

into $|\psi_{\text{iswap}}\rangle = \alpha_1|HH\rangle + i\alpha_2|VH\rangle + i\alpha_3|HV\rangle + \alpha_4|VV\rangle$, where, e.g., $|HV\rangle = |H\rangle|V\rangle = |H\rangle \otimes |V\rangle$, and $|H\rangle$ and $|V\rangle$ represent horizontal and vertical polarization states, respectively. For the sake of simplicity, we refer here to qubits encoded in photon polarization only. Obviously, we can also refer to the photon-path and phase qubits which are dual-line qubits interchangeable with polarization qubits by a polarizing beam splitter (PBS) and a beam splitter, respectively [1].

Schuch and Siewert [11] showed that the CNOT gate can be decomposed into the two iSWAP gates or the SWAP and iSWAP gates. The latter relation was also applied in [8], but not in its full power. By inverting the Schuch–Siewert relation and replacing the CNOT with the CS gate, we find that the iSWAP gate can be simply given as (see the top circuit in Fig. 1)

$$U_{\text{iSWAP}} = U_{\text{CS}}(S \otimes S)U_{\text{SWAP}}, \quad (2)$$

in terms of the phase gate $S = \text{diag}([1, i])$, the CS gate $U_{\text{CS}} = \text{diag}([1,1,1,-1])$, and the SWAP gate. The scheme can also be given in terms of the CNOT gate, as shown in

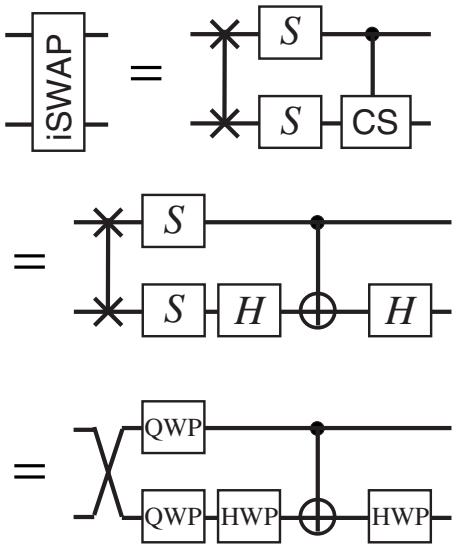

Fig. 1. Circuits decomposing the iSWAP gate into the CS and CNOT gates together with the SWAP, Hadamard (H) and phase (S) gates. The bottom scheme shows a linear-optical realization of the iSWAP using polarization-encoded qubits, where (i) the phase gate is implemented (up to a global phase factor) by a quarter-wave plate, (ii) the Hadamard gate is realized by a HWP at angle $\theta = \pi/8$, (iii) the SWAP gate can be obtained deterministically by exchanging the qubit lines, and (iv) the CS/CNOT can be realized probabilistically using one of the schemes discussed in Sections 3 and 4.

Fig. 1 (center), using the relation $U_{\text{CS}} = (I \otimes H)U_{\text{CNOT}}(I \otimes H)$. The Hadamard gate H can be implemented by the half-wave plate (HWP), which for a single qubit is given by

$$U_{\text{HWP}}(\theta) = \begin{pmatrix} \cos 2\theta & \sin 2\theta \\ \sin 2\theta & -\cos 2\theta \end{pmatrix}, \quad (3)$$

tilted at $\theta = \pi/8$.

The SWAP gate is a classical gate and can be implemented deterministically, e.g., by brute-force exchanging qubits or waveguides carrying single qubits. Using the polarization-encoded qubits, the phase gate S is simply implemented by a quarter-wave plate with a horizontal fast axis.

Note that, contrary to the iSWAP gate, the entangling power of the SWAP gate is zero, which means that this gate cannot entangle qubits, but it is just able to alter the configuration of existing entanglement among qubits. Sometimes this fact is confusing because the SWAP gate is said to have a capability of two ebits, where ebit is a unit of bipartite entanglement. This is also correct in a communication scenario. All gates except the CS (or CNOT) are deterministic, so the maximum success probability of the iSWAP is the same as those of the CS and CNOT.

The scheme of the iSWAP gate due to Wang *et al.* [8] is based on proposals by Pittman *et al.* [7] (scheme 12 in Table 1) and Zou *et al.* [4] (scheme 17) implementing the CNOT/CS gates. Scheme 17 realizing the nondestructive CS gate offers (to our knowledge) the highest probability of success (equal to 1/8) in this group of implementations using EPR states and conventional detectors as resources.

Thus, by applying scheme 17 together with the decomposition scheme shown in Fig. 1, one obtains an implementation of the iSWAP gate yielding the probability of success $P = \eta^4/8$, which is four times higher than that for the scheme of Wang *et al.* [8]. Moreover, the discussed scheme requires only eight conventional detectors instead of ten detectors used in [8]. In the next sections, we present other CNOT and CS schemes, which can be used to implement the iSWAP gate with probabilities of success equal to $\eta^4/4$, $\eta^6/8$, and $\eta^4/8$.

3. SCHEME I WITH CONVENTIONAL DETECTORS AND ANCILLAE IN GHZ STATES

Here we describe an implementation (referred to as Scheme I) of the CNOT gate based on conventional detectors and ancillae prepared in the GHZ states as shown in Fig. 2. Scheme I is obtained by combining the schemes of Gottesman and Chuang [10] (scheme 18 in Table 1) and Pittman *et al.* [7] (scheme 19). It is worth stressing that scheme 19 was originally designed solely for selective detectors. Here, we show the feasibility of the modified scheme 19 using conventional detectors. Moreover, the described scheme can be used as an implementation of the iSWAP gate according to Fig. 1.

Schemes 18 and 19 use ancilla in the following cluster-type state:

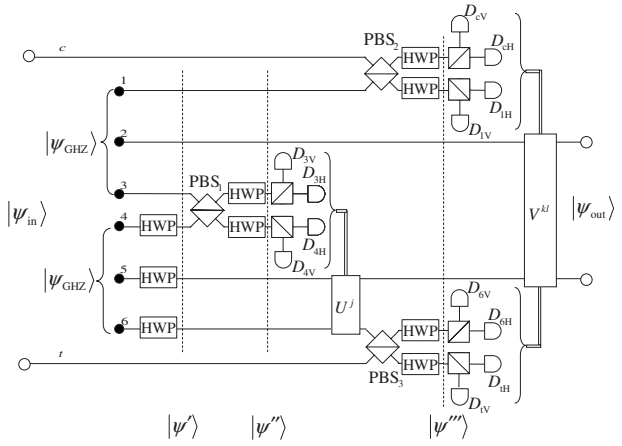

Fig. 2. Scheme I implementing the CNOT gate using conventional detectors and ancillae in the GHZ states, $|\psi_{GHZ}\rangle$. Key: HWP$=U_{HWP}(\pi/8)$ implements the Hadamard gate H; U^j and V^{kl} are conditional unitary operations given in Table 2, where σ_z is implemented by $U_{HWP}(0)$; D_k are photodetectors; PBS$_i$ are polarizing beam splitters in the HV-basis.

$$|\chi\rangle = \frac{1}{\sqrt{2}}(|HH\rangle|\Phi^+\rangle + |VV\rangle|\Psi^+\rangle), \tag{4}$$

which is equivalent (under local unitary transformations) to the standard four-qubit cluster states [12]. In Eq. (4), $|\Phi^+\rangle = \frac{1}{\sqrt{2}}(|HH\rangle + |VV\rangle)$ and $|\Psi^+\rangle = \frac{1}{\sqrt{2}}(|HV\rangle + |VH\rangle)$ are Bell's states (EPR states). Various schemes for generation of the state $|\chi\rangle$ were proposed including a nondestructive scheme [13] yielding the probability of success equal to $\eta^3/8$. It is possible to generate $|\chi\rangle$ with the success probability of $\eta^2/2$ using the Gottesman–Chuang protocol [10], which we apply in the following.

Our detailed implementation of the CNOT gate, as shown in Fig. 2, is based on schemes 18 and 19 and includes a scheme for generation of the state $|\chi\rangle$. An arbitrary input state $|\psi_{in}\rangle$, given by Eq. (1), is applied in modes c (control) and t (target). We use two ancillae in the GHZ states, $|\psi_{GHZ}\rangle = \frac{1}{\sqrt{2}}(|HHH\rangle + |VVV\rangle)$, as resources. Photons in modes 4–6 are sent through the Hadamard gate, which can be implemented by the HWP tilted at $\theta = \pi/8$ and is described by transformations $|H\rangle \to \frac{1}{\sqrt{2}}(|H\rangle + |V\rangle)$ and $|V\rangle \to \frac{1}{\sqrt{2}}(|H\rangle - |V\rangle)$. For two photons with different polarizations, the Hadamard transformation reads as $|HV\rangle \equiv |1_H 1_V\rangle \to \frac{1}{\sqrt{2}}(|2_H, 0_V\rangle - |0_H, 2_V\rangle)$. Thus, the total input state (including the ancilla states) after the action of the Hadamard gates is changed into

$$|\psi'\rangle = \frac{1}{2\sqrt{2}}(|H\rangle_1|H\rangle_2|H\rangle_3 + |V\rangle_1|V\rangle_2|V\rangle_3) \otimes (|H\rangle_4|H\rangle_5|H\rangle_6 + |V\rangle_4|V\rangle_5|H\rangle_6 + |V\rangle_4|H\rangle_5|V\rangle_6 + |H\rangle_4|V\rangle_5|V\rangle_6). \tag{5}$$

The state $|\psi'\rangle$ is sent through a polarizing beam splitter, PBS$_1$, in the HV-basis (i.e., which transmits H-polarized states and reflects V-polarized states) and the two Hadamard gates, which results in

$$|\psi''\rangle = \frac{1}{2}(|\Phi^+\rangle_{34}U^0 + |\Psi^+\rangle_{34}U^1)|\chi\rangle_{1256} + \frac{1}{2}(|V\rangle_1|V\rangle_2|\xi\rangle_3|0\rangle_4|\Phi^+\rangle_{56} + |H\rangle_1|H\rangle_2|0\rangle_3|\xi\rangle_4|\Psi^+\rangle_{56}),$$

where $U^j = (\sigma_z^{(5)} \otimes \sigma_z^{(6)})^j$ $(j = 0, 1)$ are given in terms of Pauli's matrices σ_z, $|\xi\rangle = \frac{1}{\sqrt{2}}(|2_H\rangle - |2_V\rangle)$, and $|0\rangle \equiv |0_H\rangle|0_V\rangle$ denotes no photon in H and V modes.

Whenever two photons reach separately detectors D_{3H} and D_{4H} or D_{3V} and D_{4V}, the state $|\chi\rangle$ is generated at the output (see Table 2). For combinations of single clicks at detectors D_{3H} and D_{4V} or D_{3V} and D_{4H}, the output state requires application of two Pauli's gates σ_z on photons in modes 5 and 6 to obtain the state $|\chi\rangle$. The Pauli σ_z gate can be implemented by the HWP at $\theta = 0$ according to Eq. (3).

Thus, in the discussed part of the scheme (shown in Fig. 2 up to U^j operations), it is possible to generate the state $|\chi\rangle$ after the successful postselection measurement and using feedforward. The probability of success of the generation of $|\chi\rangle$ is equal to $\eta^2/2$. The state $|\chi\rangle$ is then used as an ancilla for the CNOT gate with the input state $|\psi_{in}\rangle$, given by Eq. (1).

The state $|\psi''\rangle$ after measuring modes 3 and 4 and passing through PBS$_2$ and PBS$_3$ in the HV-basis and four HWPs is transformed into

$$|\psi'''\rangle = \frac{1}{4}[|\Phi^+\rangle_{c1}(|\Phi^+\rangle_{6t}V^{00} + |\Psi^+\rangle_{6t}V^{11}) + |\Psi^+\rangle_{c1}(|\Phi^+\rangle_{6t}V^{10} + |\Psi^+\rangle_{6t}V^{01})]|\psi_{out}\rangle_{25} + \frac{\sqrt{3}}{2}|\psi_{err}\rangle,$$

where $V^{kl} = (\sigma_z^{(2)})^k \otimes (\sigma_z^{(5)})^l$ for $k, l = 0, 1$. The state $|\psi_{err}\rangle$ is a superposition of states, which corresponds to a situation when two photons enter one pair of detectors, D_{iH} or D_{iV} for some i $(i = c, 1, 6, t)$. On the contrary, successful events are those when four photons are registered separately by all these pairs of detectors. Conventional detectors can be used because exactly four photons (without counting output photons) are always present in the setup. Other cases can be easily postselected without deteriorating the probability of success even for conventional detectors. Because of the application of Hadamard gates in front of PBSs, one can identify individual cases and use feedforward to correct the output states when it is necessary. After that one obtains $|\psi_{out}\rangle_{25} = |\psi_{cnot}\rangle$, where $|\psi_{cnot}\rangle = \alpha_1|HH\rangle + \alpha_2|HV\rangle + \alpha_3|VV\rangle + \alpha_4|VH\rangle$ as required by the CNOT operation for the input state given by Eq. (1). The probability of success of the CNOT gate is equal to $\eta^4/4$ if the state $|\chi\rangle$ is given, while the probability of success for the whole scheme shown in Fig. 2, including the generation of the state $|\chi\rangle$, accounts for $\eta^6/8$.

Finally, it is worth stressing that we treat the GHZ states as resources. These states can be obtained from, e.g., EPR-state pairs by applying a nondestructive optical method as proposed by Zeilinger *et al.* [14]. The first experimental generation of the GHZ state was realized by Bouwmeester *et al.* [15]. Since then various optical schemes for generation of the GHZ states were described

Table 2. Numbers of Photons Measured by Ideal Detectors D_i and the Corresponding Required Conditional Operations U^j and V^{kl} for Scheme I

D_{3H}	D_{3V}	D_{4H}	D_{4V}	U^j
1	0	1	0	I
0	1	0	1	I
1	0	0	1	$\sigma_z^{(5)}\otimes\sigma_z^{(6)}$
0	1	1	0	$\sigma_z^{(5)}\otimes\sigma_z^{(6)}$

D_{cH}	D_{cV}	D_{1H}	D_{1V}	D_{6H}	D_{6V}	D_{tH}	D_{tV}	V^{kl}
1	0	1	0	1	0	1	0	I
1	0	1	0	0	1	0	1	I
0	1	0	1	1	0	1	0	I
0	1	0	1	0	1	0	1	I
1	0	0	1	1	0	1	0	$\sigma_z^{(2)}$
1	0	0	1	0	1	0	1	$\sigma_z^{(2)}$
0	1	1	0	1	0	1	0	$\sigma_z^{(2)}$
0	1	1	0	0	1	0	1	$\sigma_z^{(2)}$
1	0	0	1	1	0	0	1	$\sigma_z^{(5)}$
1	0	0	1	0	1	1	0	$\sigma_z^{(5)}$
0	1	1	0	1	0	0	1	$\sigma_z^{(5)}$
0	1	1	0	0	1	1	0	$\sigma_z^{(5)}$
1	0	1	0	1	0	0	1	$\sigma_z^{(2)}\otimes\sigma_z^{(5)}$
1	0	1	0	0	1	1	0	$\sigma_z^{(2)}\otimes\sigma_z^{(5)}$
0	1	0	1	1	0	0	1	$\sigma_z^{(2)}\otimes\sigma_z^{(5)}$
0	1	0	1	0	1	1	0	$\sigma_z^{(2)}\otimes\sigma_z^{(5)}$

(see, e.g., [16–19]) and, in principle, such methods can be used to generate ancillae for Scheme I.

4. SCHEME II WITH CONVENTIONAL DETECTORS AND ANCILLAE IN EPR STATES

Here we describe an implementation of the CS gate, shown in Fig. 3 and referred to as Scheme II, using conventional detectors and ancillae in the EPR or EPR-like states. In our analysis of the experimentally oriented Scheme II, we include a few kinds of detector imperfections (dark counts, finite efficiency, and no photon-number resolution) and realistic sources of the ancilla and input states.

Our Scheme II is a modified version of the proposals by Pittman *et al.* [7] (scheme 12) and Zou *et al.* [4] (scheme 17). Note that scheme 17 was also applied by Wang *et al.* [8] as a part of their iSWAP scheme. The basic idea of Zou *et al.* [4] was to use a quantum encoder to transform an input state $\alpha|H\rangle+\beta|V\rangle$ into $\alpha|HH\rangle+\beta|VV\rangle$. The probability of success for such a device with a feedforward mechanism is equal to 1/2 (to compare with 1/4 without feedforward). In both [4,8] two such encoders (with feedforward) were used to encode an input state and to obtain finally a nondestructive gate.

Scheme II is similar to scheme 17 since it is also based on the double use of the quantum encoder and the triple use of feedforward. However, the basic idea is different: In scheme 17, output states of the encoders are measured separately. In contrast, in our scheme the output states of the encoders are combined on a PBS and only then measured. So, using this part of Scheme II one can generate a cluster-like state, while two single-qubit quantum encoders in scheme 17 can give two separate EPR pairs. Moreover, contrary to [4], we calculate the gate fidelity assuming, in particular, dark counts and realistic sources of the EPR states.

In the case of the perfect CS gate, an arbitrary pure state, given by Eq. (1), is transformed into $|\psi_{cs}\rangle=\alpha_1|HH\rangle+\alpha_2|HV\rangle+\alpha_3|VH\rangle-\alpha_4|VV\rangle$. The deviation of the output state ρ_{out} of a realistic CS gate from the state $|\psi_{cs}\rangle$ of an ideal CS gate can be described by the fidelity defined by

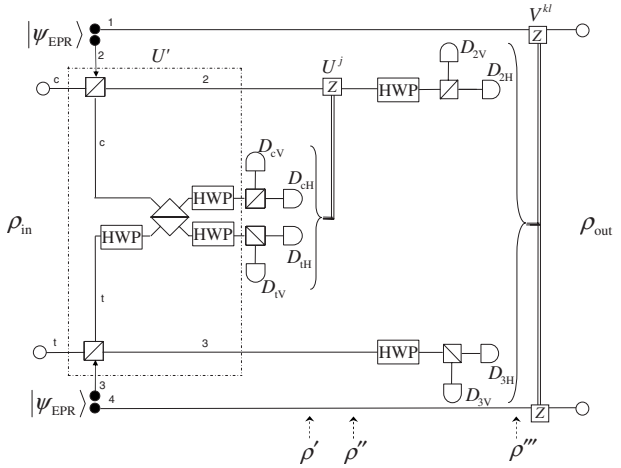

Fig. 3. Scheme II implementing the CS gate using two ancillae in perfect or non-perfect EPR states, $|\psi_{EPR}\rangle$. Notation is similar to that in Fig. 2. States and unitary operations U', U'', U^j, and V^{kl} are defined in Section 4 and in Table 3.

$$F = \langle \psi_{cs} | \rho_{out} | \psi_{cs} \rangle. \quad (6)$$

Let us first analyze the action of the multigate U' composed of six gates marked in a dotted-dashed box in Fig. 3:

$$U' = U^{(c)}_{HWP} U^{(t)}_{HWP} U^{(ct)}_{PBS} U^{(t)}_{HWP} U^{(2c)}_{PBS} U^{(t3)}_{PBS}, \quad (7)$$

where $U^{(kl)}_{PBS}$ denotes the PBS unitary transformation of k and l lines. The PBS operation in the dual-line (dual-rail) notation (and assuming labeling of lines as shown Fig. 3) corresponds to swapping of H-polarized modes and no action on V-polarized modes. $U_{HWP} = U_{HWP}(\pi/8)$ corresponds to the Hadamard gate, which can be equivalently implemented by a 50/50 beam splitter, when one of the input modes is H-polarized and the other is V-polarized, together with two $(-\pi/2)$ phase shifters [1]. The latter implementation is particularly useful to understand the Hadamard transformation applied to more than one photon.

For a moment, let us assume that the ancillae are in the perfect EPR states, $|\psi_{EPR}\rangle = |\Phi^+\rangle$. Thus, the total initial state is given by $|\Psi_{in}\rangle = |\psi_{in}\rangle_{ct} |\psi_{EPR}\rangle_{12} |\psi_{EPR}\rangle_{34}$, where $|\psi_{in}\rangle_{ct}$ is given by Eq. (1). The action of the multigate U' on the initial state $|\Psi_{in}\rangle$ can be compactly written as

$$U'|\Psi_{in}\rangle = N_{ok}|\psi_{ok}\rangle + N_{err1}|\psi_{err1}\rangle + N_{err2}|\psi_{err2}\rangle, \quad (8)$$

where $|\psi_{ok}\rangle = 1/\sqrt{2}(|\Phi^+\rangle_{ct} U^0 + |\Psi^+\rangle_{ct} U^1)|\tilde{C}_4\rangle_{1234}$ with $U^j = (\sigma_z^{(2)})^j$ $(j=0,1)$, $N^2_{ok} = 1/8$, $N^2_{err1} = (8|\alpha_1|^2 + 7|\alpha_2|^2 + 6)/16$, and $N^2_{err2} = |\alpha_2|^2/16 + (|\alpha_3|^2 + |\alpha_4|^2)/2$. In general, $|\tilde{C}_4\rangle_{1234}$ is of the form $\alpha_1|HHHH\rangle + \alpha_2|HHVV\rangle + \alpha_3|VVHH\rangle - \alpha_4|VVVV\rangle$ which, in a special case of all equal coefficients, reduces to a four-entangled cluster state $|C_4\rangle$. State $|\psi_{err1}\rangle$ corresponds to undesired cases, which *can* be excluded by measuring only modes c and t (the first postselection). In contrast, $|\psi_{err2}\rangle$ represents all the cases, in which more than one photon reaches a detector; and so, by using conventional detectors, they cannot be distinguished from one-photon states. Thus, $|\psi_{err2}\rangle$ corresponds to undesired cases, which *cannot* be uniquely excluded via the first postselection, but *can* be later excluded after measuring modes 2 and 3 (the second postselection).

It is seen that, by assuming conventional detectors without dark counts and the ancillae to be in the perfect EPR states, one obtains the probability of success equal to $P = \eta^4/8$ and the fidelity equal to 1 as in the original scheme of Zou *et al.* [4]. Note that a successful measurement corresponds to clicks of four out of eight detectors (see Table 3), which explains why $P \sim \eta^4$. Moreover, a factor of 1/8 is just equal to N^2_{ok} in Eq. (8).

So far, we presented the transformations of states by assuming perfect sources of the ancilla states and no dark counts of detectors both for Schemes I and II. Here, in contrast, we use a numerical method assuming nonperfect sources of ancillae and input states, and dark counts.

For a conventional detector of efficiency η and mean dark count rate ν, the positive-operator-valued measure (POVM) elements associated with distinguishing vacuum (Π_0) and the presence of at least one photon (Π_1) have the form

Table 3. Same as Table 2 But for Scheme II

D_{2H}	D_{2V}	D_{3H}	D_{3V}	U^j
1	0	1	0	I
0	1	0	1	I
1	0	0	1	$\sigma_z^{(2)}$
0	1	1	0	$\sigma_z^{(2)}$
D_{cH}	D_{cV}	D_{tH}	D_{tV}	V^{kl}
1	0	1	0	I
0	1	1	0	$\sigma_z^{(1)}$
1	0	0	1	$\sigma_z^{(4)}$
0	1	0	1	$\sigma_z^{(1)} \otimes \sigma_z^{(4)}$

$$\Pi_0 = \sum_{m=0}^{\infty} e^{-\nu}(1-\eta)^m |m\rangle\langle m|, \quad \Pi_1 = 1 - \Pi_0, \quad (9)$$

where $\nu = \tau_{res} R_{dark}$ is given in terms of the dark count rate, R_{dark}, and the detector resolution time τ_{res} [20].

We assume now that the entangled ancilla states are generated via spontaneous parametric downconversion (SPDC). The output state of a type-II SPDC crystal or two type-I SPDC crystals sandwiched together can be approximated as an EPR-like state of the form (see, e.g., [21,22])

$$|\psi_{EPR}\rangle = (1-\gamma^2)^{-1/2}[|0\rangle|0\rangle + \gamma(|HH\rangle + |VV\rangle)] + \mathcal{O}(\gamma^2), \quad (10)$$

where the parameter γ is given by the product of interaction time of the pump field and the crystal, their coupling constant, and complex amplitude of the pump field. The state given by Eq. (10) clearly differs from the exact EPR state $|\Phi^+\rangle$ by the inclusion of vacuum (and also higher order states) in the superposition. The parameter γ^2 is usually of the order 10^{-4}/pulse [20], and it describes the rate of single-photon pair generation per pulse of the pump field. Thus, the output state of the SPDC crystal contains vacuum with a high probability, and its effect on the gate operation cannot be neglected.

Each line in Schemes I and II can carry an arbitrary number of photons in H and V polarizations. Using a dual-line notation, one can write $|H\rangle = |1\rangle_H|0\rangle_V \equiv |1_H, 0_V\rangle$, $|V\rangle = |0\rangle_H|1\rangle_V$, and $|0\rangle = |0\rangle_H|0\rangle_V$.

The state ρ' after the action of the multigate U' and the measurement of photons by the detectors D_{cH}, D_{cV}, D_{tH}, and D_{tV} is given by

$$\rho' = \mathcal{N}\,\mathrm{Tr}_{ct}[\Pi_m^{(cH)} \Pi_{m'}^{(cV)} \Pi_n^{(tH)} \Pi_{n'}^{(tV)} U' \rho_{in} (U')^\dagger], \quad (11)$$

where $\mathrm{Tr}_{ct} \equiv \mathrm{Tr}_{cH,cV,tH,tV}$, $\rho_{in} = |\Psi_{in}\rangle\langle\Psi_{in}|$, $\mathcal{N}$ is a renormalization constant, and the POVM elements are given by Eq. (9). Moreover, m, m', n, and n' are equal to 1 or 0, corresponding to clicks or no clicks of the detectors according to Table 3. By applying the conditional gate $U^j = (\sigma_z^{(2)})^j$ with $j=0,1$, defined in Table 3, the state ρ' is transformed to $\rho'' = U^j \rho' (U^j)^\dagger$. After the operation $U'' = U^{(2)}_{HWP} U^{(3)}_{HWP}$ corresponding to the Hadamard gates at lines 2 and 3, and after photon counting by the detectors D_{2H}, D_{2V}, D_{3H}, and D_{3V}, the state ρ'' is transformed to

$$\rho''' = \mathcal{N}\,\mathrm{Tr}_{23}[\Pi_m^{(2H)}\Pi_{m'}^{(2V)}\Pi_n^{(3H)}\Pi_{n'}^{(3V)}U''\rho''(U'')^\dagger], \quad (12)$$

where $\mathrm{Tr}_{23}\equiv\mathrm{Tr}_{2H,2V,3H,3V}$, while m, n, m', and n' correspond to clicks or no clicks of the detectors according to Table 3. Note that the PBSs in front of all the detectors just convert polarization qubits into dual-line qubits, so they are redundant if we apply the dual-line notation consistently in our numerical approach. The final output state $\rho_{\mathrm{out}}=V^{kl}\rho''(V^{kl})^\dagger$ is obtained from ρ'' by applying the conditional gates $V^{kl}=(\sigma_z^{(1)})^k\otimes(\sigma_z^{(4)})^l$ $(k,l=0,1)$ according to Table 3.

For simplicity, in our numerical calculations we reserved a three-dimensional Hilbert space for each mode; thus we set $|0\rangle_H=[1;0;0]$, $|1\rangle_H=[0;1;0]$, and $|2\rangle_H=[0;0;1]$, and analogously for V polarization. This is valid by assuming dark count rates and the γ parameter to be relatively low. Otherwise, higher-dimensional Hilbert spaces should be set.

Let us assume realistic values of conventional detectors [23] (see also [20,24]): the detector efficiency is $\eta=0.7$, the dark count rate is $R_{\mathrm{dark}}=100\ \mathrm{s}^{-1}$, and the detector resolution time is $\tau_{\mathrm{res}}=10$ ns. For convenience, we assume that all detectors are the same. The rate of single-photon pair generation per pulse of the pump field is set to $\gamma^2=10^{-4}$/pulse [20]. For experimental verification of Scheme II, it is useful to assume that the input state $|\psi_{\mathrm{in}}\rangle$ is also generated by the SPDC and is given by Eq. (10). For brevity, we analyze only the first cases in Table 3, where no extra conditional operations are required. Under these assumptions, we find that the fidelity drops to $F\approx 0.97$, which is still relatively high.

5. CONCLUSIONS

We studied linear-optical implementations of two-qubit universal gates including the iSWAP and CS/CNOT gates. As shown in Table 1, the majority of these realizations of nondestructive gates are based on single-photon detectors. In contrast, we focused on practical implementations using conventional detectors, which do not resolve a number of photons.

Despite the progress in constructing single-photon detectors (see [25,26] and references therein), they are still not commonly used. This conclusion can be drawn, e.g., by analyzing experimental realizations of quantum gates listed in Table 1. One of the drawbacks of single-photon detectors is that their dark count rates are much higher than those for conventional detectors [26]. There are also proposals of multiple-photon resolving detectors including cascade arrays of conventional detectors (connected with beam splitters or with high-speed low-loss optical switches [27]) and fiber-loop detectors [28]. Such detectors, which are based on the idea of chopping up photons, are conceptually very attractive but still experimentally underdeveloped.

We analyzed a recent proposal of Wang *et al.* [8] to implement the iSWAP gate using two entangled ancillae in EPR states, classical feedforward, and conventional photodetectors (of a finite efficiency η) with the success probability of $\eta^4/32$ only. This scheme was based on an implementation of the CS gate by Zou *et al.* [4] (scheme 17 in Table 1) with the success probability of $\eta^4/8$.

We showed that the iSWAP gate can be decomposed into the CS/CNOT gate and deterministic gates including the SWAP, phase, or Hadamard gates. Thus, one can immediately obtain schemes that implement the iSWAP gate by using the CS/CNOT gates with relatively high probabilities of success. In particular, by applying scheme 17 of Zou *et al.* [4] together with the iSWAP decomposition scheme, we showed how to implement the iSWAP gate with the success probability four times higher than that in the scheme of Wang *et al.* [8].

Moreover, we studied the applicability of conventional detectors to other implementations of nondestructive gates originally designed for single-photon detectors. We showed that the scheme of Pittman *et al.* [7] implementing the nondestructive CNOT gate can be used also with conventional detectors achieving the probability of success equal to $\eta^4/4$ assuming as a resource the Gottesman–Chuang four-qubit entangled state [10] or equal to $\eta^6/8$ for a pair of ancillae in the GHZ states.

We have also described another scheme based on conventional detectors and ancillae in the EPR or EPR-like states as a modified version of the scheme by Zou *et al.* [4]. To verify the experimental feasibility of this scheme, we showed how the quantum gate fidelity is deteriorated due to realistic sources of ancilla and input states, and detector imperfections to include dark counts, finite efficiency, and no photon-number resolution.

APPENDIX A: COMPARISON OF THE SCHEMES LISTED IN TABLE 1

Here, we give more explanations and compare various linear-optical implementations of the CS/CNOT gates listed in Table 1. Obviously, these schemes can be used also to construct the iSWAP gate according to Fig. 1. The implementations can be divided into several groups according to, e.g., different resources as shown in Table 1: (I) unentangled ancillae, (II) entangled ancillae, and (III) without ancillae at all. Our examples of the second group include not only ancillae in the EPR states described in Section 4, but also the Gottesman–Chuang four-entangled state and the GHZ states discussed in Section 3.

We compared the schemes concerning the total probability of success, destructive or nondestructive character of the implementations, application of conventional or nonconventional detectors, and whether the feedforward mechanism was applied. Classical feedforward means that a scheme includes measurement devices of some modes such that the classical outcomes of the measurements can be used to change the remaining modes.

In group I, where one or two ancillae prepared in an unentangled state were used, the highest probability of success for the gates without feedforward accounts for 2/27 [29] (for scheme 3 in Table 1). It is worth noting that there is only numerical evidence [30], but no analytical proof (contrary, e.g., to the nonlinear sign shift gate [31]) that 2/27 is the rigorous tight upper bound on the success probability using two unentangled ancillae without feedforward. Moreover, additional ancillae do not increase this value. When feedforward is used the probability can be increased to 1/8 for gates with two ancillae [32,33]

(schemes 6 and 7) or even to 1/4 with one ancilla [34] (schemes 4 and 5) at the expense of destructing the output states. It should be mentioned that for all these groups of implementations, the destructive gates (i.e., those for which *not* only ancilla states are measured) achieve higher probabilities.

In group II, the best achieved probability of success accounts for 1/16 without feedforward [3,7] (schemes 9 and 12) and 1/4 with feedforward [2,7,32] (schemes 8, 13, and 16).

Group III consists of the CS/CNOT gates based on the idea of Hofmann and Takeuchi [35] (scheme 25) and Ralph *et al.* [36] (scheme 26). Other examples in this group are mainly experimental realizations of schemes 25 and 26 using a beam splitter with the reflection coefficient equal to 1/3. The probability of success for them achieves 1/9, assuming the measurement of both the control and target bits for the postselection.

Intentionally, we have not included implementations of the CS/CNOT gates based on the idea of one-way computation using cluster states as proposed by Raussendorf and Briegel [12]. According to their proposal one can implement the CS/CNOT gate by performing single-qubit measurement in an appropriate basis on a given cluster state. Using this procedure with additional feedforward it is possible to implement the CS/CNOT gate nearly deterministically even with conventional detectors as described, e.g., in [37–40] and experimentally realized in [41–44].

However, it should be stressed that such implementations of the CS/CNOT gates based on cluster-type states look deterministic only, because it is assumed something strictly easier than applying the true CNOT gate on *independently* prepared input photonic qubits. The latter task should not be deterministic because of the no-go theorem for the Bell measurement by linear optics.

It is worth clarifying that Table 1 includes two schemes using the cluster-type states. Namely, schemes of Gottesman and Chuang [10] (scheme 18) and closely related proposal of Pittman *et al.* [7] (scheme 19) are implementations of the nondestructive and nondeterministic CNOT gate using a four-photon entangled state $|\chi\rangle$, which is equivalent, under a local unitary transformation, to a four-qubit cluster state. We included this gate in Table 1 since it does not realize the Raussendorf–Briegel protocol, but uses the state $|\chi\rangle$ as an ancilla only.

In Table 1, we also have not included deterministic implementations of the universal gates based on single-photon cross-Kerr nonlinearities (see [1,45] and references therein). Such schemes are fundamentally different from probabilistic linear-optical schemes. Moreover, there are serious doubts [46] on whether they can be useful for quantum computing if applied for single photons in a standard way.

ACKNOWLEDGMENTS

The authors thank Nobuyuki Imoto, Bryan Jacobs, Masato Koashi, and Zhi Zhao for discussions. The work was supported by the Polish Ministry of Science and Higher Education under Grant No. 2619/B/H03/2010/38.

REFERENCES

1. P. Kok, W. J. Munro, K. Nemoto, T. C. Ralph, J. P. Dowling, and G. J. Milburn, "Linear optical quantum computation with photonic qubits," Rev. Mod. Phys. **79**, 135–174 (2007).
2. E. Knill, R. Laflamme, and G. J. Milburn, "A scheme for efficient quantum computation with linear optics," Nature **409**, 46–52 (2001).
3. M. Koashi, T. Yamamoto, and N. Imoto, "Probabilistic manipulation of entangled photons," Phys. Rev. A **63**, 030301(R) (2001).
4. X. Zou, S. Zhang, K. Li, and G. Guo, "Linear optical implementation of the two-qubit controlled phase gate with conventional photon detectors," Phys. Rev. A **75**, 034302 (2007).
5. S. Gasparoni, J. W. Pan, P. Walther, T. Rudolph, and A. Zeilinger, "Realization of a photonic controlled-NOT gate sufficient for quantum computation," Phys. Rev. Lett. **93**, 020504 (2005).
6. Z. Zhao, A. N. Zhang, Y. A. Chen, H. Zhang, J. F. Du, T. Yang, and J. W. Pan, "Experimental demonstration of a nondestructive controlled-NOT quantum gate for two independent photon qubits," Phys. Rev. Lett. **94**, 030501 (2004).
7. T. B. Pittman, B. C. Jacobs, and J. D. Franson, "Probabilistic quantum logic operations using polarizing beam splitters," Phys. Rev. A **64**, 062311 (2001).
8. H. F. Wang, X. Q. Shao, Y. F. Zhao, S. Zhang, and K. H. Yeon, "Scheme for implementing linear optical quantum iSWAP gate with conventional detectors," J. Opt. Soc. Am. B **27**, 27–31 (2010).
9. T. Tanamoto, K. Maruyama, Y. X. Liu, X. Hu, and F. Nori, "Efficient purification protocols using iSWAP gates in solid-state qubits," Phys. Rev. A **78**, 062313 (2008).
10. D. Gottesman and I. L. Chuang, "Demonstrating the viability of universal quantum computation using teleportation and single-qubit operations," Nature **402**, 390–393 (1999).
11. N. Schuch and J. Siewert, "Natural two-qubit gate for quantum computation using XY interaction," Phys. Rev. A **67**, 032301 (2003).
12. R. Raussendorf and H. J. Briegel, "A one-way quantum computer," Phys. Rev. Lett. **86**, 5188–5191 (2001).
13. H. F. Wang and S. Zhang, "Scheme for linear optical preparation of a type of four-photon entangled state with conventional photon detectors," Eur. Phys. J. D **53**, 359–363 (2009).
14. A. Zeilinger, M. A. Horne, H. Weinfurter, and M. Zukowski, "Three-particle entanglements from two entangled pairs," Phys. Rev. Lett. **78**, 3031–3034 (1997).
15. D. Bouwmeester, J. W. Pan, M. Daniell, H. Weinfurter, and A. Zeilinger, "Observation of three photon Greenberger–Horne–Zeilinger entanglement," Phys. Rev. Lett. **82**, 1345–1349 (1999).
16. X.-F. Fan, T. Yang, J. Li, C. F. Li, and G. C. Guo, "Generation three-particle entanglement states," Phys. Lett. A **284**, 59–62 (2001).
17. Y. Sagi, "Scheme for generating Greenberger–Horne–Zeilinger-type states of n photons," Phys. Rev. A **68**, 042320 (2003).
18. F. Shafiei, P. Srinivasan, and Z. Y. Ou, "Generation of three-photon entangled state by quantum interference between a coherent state and parametric down-conversion," Phys. Rev. A **70**, 043803 (2004).
19. H.-X. Lu, J. Zhang, X.-Q. Wang, Y.-D. Li, and C.-Y. Wang, "Experimental high-intensity three-photon entangled source," Phys. Rev. A **78**, 033819 (2008).
20. S. K. Özdemir, A. Miranowicz, M. Koashi, and N. Imoto, "Quantum scissors device for optical state truncation: a proposal for practical realization," Phys. Rev. A **64**, 063818 (2001).
21. A. Gilchrist, W. J. Munro, and A. G. White, "Input states for quantum gates," Phys. Rev. A **67**, 040304(R) (2003).
22. C. Gerry and P. Knight, *Introductory Quantum Optics* (Cambridge U. Press, 2004).
23. Data sheet on SPCM-AQ photon-counting module, EG&G, Optoelectronics Division, Vaudreuil, Canada.
24. A. Miranowicz, "Optical-state truncation and teleportation

of qudits by conditional eight-port interferometry," J. Opt. B: Quantum Semiclassical Opt. **7**, 142–150 (2005).
25. "Special issue on single-photon detectors," J. Mod. Opt. **51**, 1265–1557 (2004).
26. S. Takeuchi, J. Kim, Y. Yamamoto, and H. H. Hogue, "Development of a high-quantum-efficiency single-photon counting system," Appl. Phys. Lett. **74**, 1063–1065 (1999).
27. S. A. Castelletto, I. P. Degiovanni, V. Schettini, and A. L. Migdall, "Reduced deadtime and higher rate photon-counting detection using a multiplexed detector array," J. Mod. Opt. **54**, 337–352 (2007).
28. J. Řeháček, Z. Hradil, O. Haderka, J. Peřina, Jr., and M. Hamar, "Multiple-photon resolving fiber-loop detector," Phys. Rev. A **67**, 061801(R) (2003).
29. E. Knill, "Quantum gates using linear optics and postselection," Phys. Rev. A **66**, 052306 (2002).
30. D. B. Uskov, L. Kaplan, A. M. Smith, S. D. Huver, and J. P. Dowling, "Maximal success probabilities of linear-optical quantum gates," Phys. Rev. A **79**, 042326 (2009).
31. J. Eisert, "Optimizing linear optics quantum gates," Phys. Rev. Lett. **95**, 040502 (2005).
32. G. L. Giorgi, F. de Pasquale, and S. Paganelli, "Conditional sign flip via teleportation," Phys. Rev. A **70**, 022319 (2004).
33. X. H. Bao, T. Y. Chen, Q. Zhang, J. Yang, H. Zhang, T. Yang, and J. W. Pen, "Optical nondestructive controlled-NOT gate without using entangled photons," Phys. Rev. Lett. **98**, 170502 (2007).
34. T. B. Pittman, M. J. Fitch, B. C. Jacobs, and J. D. Franson, "Experimental controlled-NOT logic gate for single photons in the coincidence basis," Phys. Rev. A **68**, 032316 (2003).
35. H. F. Hofmann and S. Takeuchi, "Quantum phase gate for photonic qubits using only beam splitters and postselection," Phys. Rev. A **66**, 024308 (2002).
36. T. C. Ralph, N. K. Langford, T. B. Bell, and A. G. White, "Linear optical controlled-NOT gate in the coincidence basis," Phys. Rev. A **65**, 062324 (2002).
37. M. A. Nielsen, "Optical quantum computation using cluster states," Phys. Rev. Lett. **93**, 040503 (2004).
38. D. E. Browne and T. Rudolph, "Resource-efficient linear optical quantum computation," Phys. Rev. Lett. **95**, 010501 (2005).
39. Y. Tokunaga, T. Yamamoto, M. Koashi, and N. Imoto, "Simple experimental scheme of preparing a four-photon entangled state for the teleportation-based realization of a linear optical controlled-NOT gate," Phys. Rev. A **71**, 030301(R) (2005).
40. N. Yoran and B. Resnik, "Deterministic linear optics quantum computation with single photon qubits," Phys. Rev. Lett. **91**, 037903 (2003).
41. P. Walther, K. J. Resch, T. Rudolph, E. Schenck, H. Weinfurter, V. Vedral, M. Aspelmeyer, and A. Zeilinger, "Experimental one-way quantum computing," Nature **434**, 169–176 (2005).
42. N. Kiesel, Ch. Schmid, U. Weber, G. Tóth, O. Gühne, R. Ursin, and H. Weinfurter, "Experimental analysis of a four-qubit photon cluster state," Phys. Rev. Lett. **95**, 210502 (2005).
43. Y. Tokunaga, S. Kuwashiro, T. Yamamoto, M. Koashi, and N. Imoto, "Generation of high-fidelity four-photon cluster state and quantum-domain demonstration of one-way quantum computing," Phys. Rev. Lett. **100**, 210501 (2008).
44. W. B. Gao, P. Xu, X. C. Yao, O. Gühne, A. Cabello, C. Y. Lu, C. Z. Peng, Z. B. Chen, and J. W. Pan, "Experimental realization of a controlled-NOT gate with four-photon six-qubit cluster states," Phys. Rev. Lett. **104**, 020501 (2010).
45. K. Nemoto and W. J. Munro, "Nearly deterministic linear optical controlled-NOT gate," Phys. Rev. Lett. **93**, 250502 (2004).
46. J. H. Shapiro, "Single-photon Kerr nonlinearities do not help quantum computation," Phys. Rev. A **73**, 062305 (2006).
47. T. C. Ralph, A. G. White, W. J. Munro, and G. J. Milburn, "Simple scheme for efficient linear optics quantum gates," Phys. Rev. A **65**, 012314 (2001).
48. T. B. Pittman, B. C. Jacobs, and J. D. Franson, "Demonstration of nondeterministic quantum logic operations using linear optical elements," Phys. Rev. Lett. **88**, 257902 (2002).
49. J. L. O'Brien, G. J. Pryde, A. G. White, T. C. Ralph, and D. Branning, "Demonstration of an all-optical quantum controlled-NOT gate," Nature **426**, 264–267 (2003).
50. R. Okamoto, H. F. Hofmann, S. Takeuchi, and K. Sasaki, "Demonstration of an optical quantum controlled-NOT gate without path interference," Phys. Rev. Lett. **95**, 210506 (2005).
51. N. Kiesel, Ch. Schmid, U. Weber, R. Ursin, and H. Weinfurter, "Linear optics controlled-phase gate made simple," Phys. Rev. Lett. **95**, 210505 (2005).
52. N. K. Langford, T. J. Weinhold, R. Prevedel, K. L. Resh, A. Gilchrist, J. L. O'Brien, G. J. Pryde, and A. G. White, "Demonstration of a simple entangling optical gate and its use in Bell-state analysis," Phys. Rev. Lett. **95**, 210504 (2005).